ICASSP 2024 - 2024 IEEE International Conference on Acoustics, Speech and Signal Processing (ICASSP) | 979-8-3503-4485-1/24/$31.00 ©2024 IEEE | DOI: 10.1109/ICASSP48485.2024.10446447

USING TEMPORAL CONSISTENCY FOR COMPRESSED SENSING IN HIGH-RESOLUTION MMWAVE SOUNDING

S. Semper*,†, J. Chuang†, S. Berweger†, C. Gentile†
* Technische Universität Ilmenau, EMS, Ilmenau, Germany;
† Radio Access and Propagation Metrology Group, National Institute of Standards and Technology, Gaithersburg, MD 20899-6730 USA

ABSTRACT

Switched phased array systems operating at high sample rates generate large amounts of data during measurements of radio channels, but many scenarios contain only few multipath components. Compressed Sensing suggests in these cases Nyquist-rate samples are wasteful in terms of data size. It has been observed that structural parameters, i.e., time of flight and angle of arrival, of the propagation paths are temporally consistent, as they vary slowly in time.

Hence, we propose a local temporally consistent signal model that includes delay and angle of arrival, and also their time-derivatives, coherently connecting multiple radio channel snapshots. This allows to use a cyclic compression scheme consisting of a few compression matrices that extract mutually incoherent information from adjacent snapshots. Last, we present an algorithm to extract specular multipath components from these compressive measurements.

We verify our findings on simulated data and real measurements. On simulated data we observe a good agreement of the estimates with the available ground-truth and show that the proposed cyclic compression scheme improves estimation accuracy. On measured data, we compare the estimates from data obtained at Nyquist rate to data compressed to $17\,\%$ of the original size and find good agreement as well.

Keywords: *mmWave, Compressed Sensing, Sparse Signal Recovery*

I. INTRODUCTION

To derive channel models for mmWave sensing and beyond, high bandwidth channel sounders are used to conduct the necessary measurements. For many sensing applications the expected number of Multipath Components (MPCs) is low, i.e. the observed radio channels allow a sparse approximation. Additionally, the high data rates are not used for resolving a high number MPCs, but rather to provide high resolution to better differentiate MPCs in the estimated domains, e.g., delay and Angle of Arrival (AoA) as considered in this work. For example, the mmWave sounding system presented in [1] uses switched beamforming to acquire channel measurements. In contrast to conventional beamforming, a switched beamforming scheme rapidly switches through the receive antennas without any phase shifts applied, which greatly reduces the overall measurement time. The beamforming is then conducted digitally in the estimation procedure. The system is equipped with 256 dual polarized receive elements and stores single precision complex impulse responses of size $16\,376$, which amounts to at least $68\,\mathrm{MB}$ of data per snapshot, if we only acquire a single impulse response. At a snapshot rate of $385\,\mathrm{Hz}$ this accumulates $26\,\mathrm{GB}$ of data per second of measurement duration. Hence, for campaigns lasting more than a few seconds, memory limitation quickly becomes an issue.

After measurements, recovery of MPC parameters can be achieved efficiently by greedy and iterative methods like CLEAN, Space-Alternating Generalized Expectation-Maximization (SAGE) [2] or RIMAX [3]. These approaches approximate a solution to the maximum likelihood problem and are able to incorporate different device and propagation models, allowing super-resolution [4].

The theory of Compressed Sensing (CS) provides a framework to reduce the data storage requirements while still allowing for super-resolution [5]–[7], which in the context of channel sounding means using the sparsity of the radio channel due to the low number of specular reflections [8].

Not only is the radio channel sparse, but over time the parameters are slowly time-varying [9]. If we consider a measurement campaign consisting of possibly thousands of snapshots, this means that temporally adjacent snapshots are highly correlated. This suggests that we can impose temporal consistency for a more expressive signal model, for instance by incorporating the rates of change of the MPC parameters. It should also be possible to devise a compression scheme that delivers uncorrelated observations from correlated snapshots, which intuitively should retain more information in the compressed data. It is the goal of this paper to deduce how such an approach might be devised, implemented, and evaluated.

In [10] the authors consider AoA estimation using Fast Iterative Shrinkage-Thresholding Algorithm (FISTA) and a successive refinement by SAGE to provide a sparse recovery scheme for channel sounding. However, no compression scheme, no temporal consistency, and no experiments on measurement are presented. The work in [8] simulatively studies the effect of compression on the obtainable mean squared error (MSE) based on parameters extracted from real measurement campaigns, but no temporal information is used and the publication conducts no estimates based on the devised compression schemes. The authors of [11] present a grid-free maximum likelihood estimator from compressed data based on gradient iterations. However, the experiments solely rely on simulated data and neglect the temporal consistency when processing successive snapshots. Similarly to our proposal, the authors in [9] also use a state-space formulation for the tracking of MPC parameters that also incorporates rates of change. However compressed sensing is not considered therein.

Based on this, the contributions of our work are as follows. We propose to use a parametric model that allows a local approximation to account for the temporal consistency of the MPCs' parameters. Also, we propose to use a cyclic compression scheme consisting of a finite set of measurement matrices that allow processing in realistic sounding measurement campaigns while making use of the introduced spatial consistency. Additionally, we introduce a possible parameter estimation routine that incorporates both concepts into a complete processing pipeline. Finally, we verify our approach based on numerical experiments applied to both synthetic and real measurements from a mmWave channel sounder [1].

In this manuscript we use S^2 to denote the manifold of the unit sphere in $\mathbb{R}^3$ and $\mathbb{T}S^2$ as its tangent bundle. Let $\boldsymbol{I}_n$ denote the identity matrix, on $\mathbb{R}^n$ and let $\mathbf{E}(X)$ denote the expectation of a possibly matrix-valued random variable X. We use $\|\cdot\|_F$ to denote the Frobenius norm and $\jmath$ is the imaginary unit. Moreover, δ_{ij} is the Kronecker delta symbol that is unity when $i = j$ and zero otherwise. Bold-faced variables denote either vectors or matrices.

This work is partly funded by the DFG projects HoPaDyn with Grant-No. TH 494/30-1 and JCRSP CoMP with Grant-No. TH 494/35-1

Authorized licensed use limited to: NIST Virtual Library (NVL). Downloaded on July 14,2025 at 16:48:16 UTC from IEEE Xplore. Restrictions apply.

II. Signal Model

A. Uncompressed Signal Model

Assume there are $P \in \mathbb{N}$ narrow-band single-polarized plane waves impinging at an array of antennas with $N_{\mathrm{rx}} \in \mathbb{N}$ output ports, where these waves originate from transmitting the bandlimited complex base-band waveform $x : \mathbb{R} \to \mathbb{C}$. Then, the complex vector-valued receive signal $\boldsymbol{y} : \mathbb{R} \to \mathbb{C}^{N_{\mathrm{rx}}}$ can be modeled as

$$\boldsymbol{y}(t) = \sum_{p=1}^{P} \gamma_p \cdot x(t - \tau_p) \cdot \exp\left[-\jmath \cdot 2\pi \cdot \boldsymbol{\varphi}(\Omega_p)\right]. \tag{1}$$

Here, $\boldsymbol{\varphi} : S^2 \to \mathbb{R}^{N_{\mathrm{rx}}}$ represents the phase-shifts stemming from the angle of arrival $\Omega_p \in S^2$ of the p-th MPC and the distances of the individual antenna ports to the antenna's phase center. Moreover, τ_p represents the delay of the p-th MPC and $\gamma_p \in \mathbb{C}$ is its path-weight.

We obtain $N_t \in \mathbb{N}$ samples of $\boldsymbol{y}$ and hence a critically sampled version $\boldsymbol{Y} \in \mathbb{C}^{N_{\mathrm{rx}} \times N_{\mathrm{t}}}$ of $\boldsymbol{y}$ as

$$\boldsymbol{Y} = \sum_{p=1}^{P} \gamma_p \cdot \exp\left[-\jmath \cdot 2\pi \cdot \boldsymbol{\varphi}(\Omega_p)\right] \cdot \boldsymbol{\mathcal{S}}(\tau_p)\{\boldsymbol{x}\}^{\mathrm{T}}, \tag{2}$$

where $\boldsymbol{x} \in \mathbb{C}^{N_{\mathrm{t}}}$ is the sampled version of the sending signal x and $\boldsymbol{\mathcal{S}}(\tau)$ is the linear shift operator by delay $\tau \in \mathbb{R}$, which transforms a discretized signal into the signal that is first shifted and then discretized. We assume that the sampling of $\boldsymbol{Y}$ is carried out within the radio channel's coherence time, such that the effect of the switched beamforming can be neglected. Note that above notation does not necessarily assume that we obtain a Nyquist-sampled observation of $\boldsymbol{y}$. We use the discretized notation only for notational convenience offered by finite dimensional vector algebra. The sparsity of $\boldsymbol{Y}$ is obvious from the fact that for practical scenarios, we have that $P \ll N_{\mathrm{rx}} N_{\mathrm{t}}$.

B. Compressed Signal Model

To continue we define $\boldsymbol{f} : \mathbb{R} \to \mathbb{C}^{N_{\mathrm{t}}}$ as $\tau \mapsto \boldsymbol{\mathcal{S}}(\tau)\{\boldsymbol{x}\}$ and $\boldsymbol{s} : S^2 \to \mathbb{C}^{N_{\mathrm{rx}}}$ as $\Omega \mapsto \exp\left[-\jmath \cdot 2\pi \cdot \boldsymbol{\varphi}(\Omega)\right]$. Next, we introduce two compression matrices $\boldsymbol{\Phi} \in \mathbb{C}^{m_{\mathrm{rx}} \times N_{\mathrm{rx}}}$ and $\boldsymbol{\Psi} \in \mathbb{C}^{m_{\mathrm{t}} \times N_{\mathrm{t}}}$. With these we obtain a compressed observation $\boldsymbol{Z} \in \mathbb{C}^{m_{\mathrm{rx}} \times m_{\mathrm{t}}}$ as

$$\boldsymbol{Z} = \boldsymbol{\Phi} \boldsymbol{Y} \boldsymbol{\Psi}^{\mathrm{T}} = \sum_{p=1}^{P} \gamma_p \{\boldsymbol{\Phi}\boldsymbol{s}\}(\Omega_p)\{\boldsymbol{\Psi}\boldsymbol{f}\}(\tau_p)^{\mathrm{T}}, \tag{3}$$

resulting in the same Kronecker, i.e. Khatri-Rao, structure as the data model (2). As such, $\boldsymbol{\Phi}$ represents the spatial compression, while $\boldsymbol{\Psi}$ represents the temporal compression. This gives a parametric model mapping from $\boldsymbol{\gamma} = (\gamma_1, \ldots, \gamma_P) \in \mathbb{C}^P$, $\boldsymbol{\tau} = (\tau_1, \ldots, \tau_P) \in \mathbb{R}^P$ and $\boldsymbol{\Omega} = (\Omega_1, \ldots, \Omega_1) \in \{S^2\}^P$ to the compressed observation $\boldsymbol{Z}(\boldsymbol{\gamma}, \boldsymbol{\tau}, \boldsymbol{\Omega})$.

C. Compressed Window Model

In a real measurement campaign, we observe a series of snapshots $(\boldsymbol{S}_k)_{k \in \mathbb{N}}$ following the parametric models of $\boldsymbol{Z}$. It has been empirically observed that between the observations $\boldsymbol{S}_k$ and $\boldsymbol{S}_{k+1}$ the delay and AoA parameters of the MPCs do not change drastically, since the time gap between measurements is in the range of a few milliseconds. Hence, if we consider observation $k \in \mathbb{N}$ and $\boldsymbol{\tau}_k, \dot{\boldsymbol{\tau}}_k \in \mathbb{R}^P$ and $\boldsymbol{\Omega}_k \in \{S^2\}^P$, $\dot{\boldsymbol{\Omega}}_k \in (\mathbb{T}S^2)^P$ denote Time-of-Flights (ToFs) and their rates of change and the Direction of Arrivals (DoAs), respectively, we can make the following local linear approximations,

$$\boldsymbol{\tau}_{k+\ell} \approx \boldsymbol{\tau}_k + \ell \cdot \dot{\boldsymbol{\tau}}_k \quad \text{and} \quad \boldsymbol{\Omega}_{k+\ell} \approx \boldsymbol{\Omega}_k + \ell \cdot \dot{\boldsymbol{\Omega}}_k, \tag{4}$$

where $|\ell| \leqslant L$ is the time step between adjacent observations for some $L \in \mathbb{N}$. Now we can make the following approximation for the observations by considering the parameters of snapshot k, i.e. $\boldsymbol{\tau}_k$, $\dot{\boldsymbol{\tau}}_k$, $\boldsymbol{\Omega}_k$ and $\dot{\boldsymbol{\Omega}}_k$, via

$$\boldsymbol{S}_{k+\ell} \approx \boldsymbol{Z}(\boldsymbol{\gamma}_{k+\ell}, \boldsymbol{\tau}_k + \ell \cdot \dot{\boldsymbol{\tau}}_k, \boldsymbol{\Omega}_k + \ell \cdot \dot{\boldsymbol{\Omega}}_k) = \boldsymbol{Z}_\ell. \tag{5}$$

Hence, (5) represents a local parametric model that, given an $L \in \mathbb{N}$, allows to construct the mapping

$$(\boldsymbol{\gamma}_{k-L}, \ldots, \boldsymbol{\gamma}_{k+L}, \boldsymbol{\tau}_k, \dot{\boldsymbol{\tau}}_k, \boldsymbol{\Omega}_k, \dot{\boldsymbol{\Omega}}_k) \mapsto (\boldsymbol{Z}_{-L}, \ldots, \boldsymbol{Z}_{+L}), \tag{6}$$

which constitutes a parametric model connecting $2L + 1$ consecutive observations as a single observation window enforcing continuity by use of the rates of change $\dot{\boldsymbol{\tau}}$ and $\dot{\boldsymbol{\Omega}}$. We note that we refrain from applying such a local approximation to the complex pathweights $\boldsymbol{\gamma}$, since the complex phases, especially for higher frequencies, obey a much weaker temporal consistency than the delay and AoA.

D. Cyclic Compression Scheme

Since adjacent snapshots $\boldsymbol{S}_k$ and $\boldsymbol{S}_{k+\ell}$ for $|\ell| \leqslant L$ are modeled consistently by (6), we can increase the information obtained from the channel by using individual compression matrices $\boldsymbol{\Phi}_k$, $\boldsymbol{\Phi}_{k+\ell}$ and $\boldsymbol{\Psi}_k$, $\boldsymbol{\Psi}_{k+\ell}$, respectively, to obtain $\boldsymbol{S}_k$ and $\boldsymbol{S}_{k+\ell}$.

However, using every compression matrix only once during a measurement campaign would be impractical because they also have to be stored along with the sequence $(\boldsymbol{S}_k)_{k \in \mathbb{N}}$, essentially eliminating the data storage reduction. Our local model (6) only assumes consistency across $2L+1$ consecutive $\boldsymbol{S}_k$. As a consequence, it is enough to only construct $2L + 1$ different compression matrices of $\tilde{\boldsymbol{\Phi}}_k$ and $\tilde{\boldsymbol{\Psi}}_k$ respectively and reuse them in a cyclic fashion by setting

$$\boldsymbol{\Phi}_k = \tilde{\boldsymbol{\Phi}}_{k \mod 2L+1} \quad \text{and} \quad \boldsymbol{\Psi}_k = \tilde{\boldsymbol{\Psi}}_{k \mod 2L+1}.$$

for the usage in (3).

Finally, we draw the entries of $\tilde{\boldsymbol{\Phi}}_k$ and $\tilde{\boldsymbol{\Psi}}_k$ identically and uniformly distributed from the set $\{+1, -1, +\jmath, -\jmath\}$. These have been observed to be well suited as compression matrices [12], only need addition and subtraction during multiplication with a vector and they satisfy

$$\mathbf{E}\left(\tilde{\boldsymbol{\Phi}}_k \cdot \tilde{\boldsymbol{\Phi}}_j^{\mathrm{H}}\right) = \delta_{kj} N_{\mathrm{rx}} \boldsymbol{I} \quad \text{and} \quad \mathbf{E}\left(\tilde{\boldsymbol{\Psi}}_k \cdot \tilde{\boldsymbol{\Psi}}_j^{\mathrm{H}}\right) = \delta_{kj} N_{\mathrm{t}} \boldsymbol{I},$$

which is exactly the property we desire when aiming at extracting complementary information in adjacent snapshots.

III. Estimation Procedure

In order to solve the inverse problem that recovers the parameters from the time-series of observations $(\boldsymbol{S}_k)_{k \in \mathbb{N}}$, we invoke the maximum likelihood principle due to its advantageous properties in terms of efficiency and sufficiency.

A. Maximum Likelihood

Under the assumption of additive Gaussian white noise $\boldsymbol{N} \in \mathbb{C}^{N_{\mathrm{rx}} \times N_t}$ with variance $\sigma^2 > 0$, we observe

$$\boldsymbol{S}_k = \boldsymbol{Z}(\boldsymbol{\theta}_k) + \boldsymbol{\Phi} \cdot \boldsymbol{N} \cdot \boldsymbol{\Psi}^{\mathrm{T}}$$

and the negative log-likelihood function based on (6) is

$$\lambda(\boldsymbol{\theta}_k | \boldsymbol{S}_{k-L}, \ldots, \boldsymbol{S}_{k+L}) \sim \sigma^{-2} \sum_{\ell=-L}^{+L} \|\boldsymbol{Z}_\ell(\boldsymbol{\theta}_{k,\ell}) - \boldsymbol{S}_{k+\ell}\|_F^2 \tag{7}$$

up to constant, i.e. independent of $\boldsymbol{\theta}_k$, summands. Here, we have used the abbreviations

$$\boldsymbol{\theta}_{k,\ell} = (\boldsymbol{\gamma}_{k+\ell}, \boldsymbol{\tau}_k, \dot{\boldsymbol{\tau}}_k, \boldsymbol{\Omega}_k, \dot{\boldsymbol{\Omega}}_k).$$

and

$$\boldsymbol{\theta}_k = (\boldsymbol{\gamma}_{k-L}, \ldots, \boldsymbol{\gamma}_{k+L}, \boldsymbol{\tau}_k, \dot{\boldsymbol{\tau}}_k, \boldsymbol{\Omega}_k, \dot{\boldsymbol{\Omega}}_k). \tag{8}$$

The maximum likelihood approach aims to recover an estimate $\hat{\boldsymbol{\theta}}_k$ by solving

$$\hat{\boldsymbol{\theta}}_k = \operatorname*{argmin}_{\boldsymbol{\theta}} \lambda(\boldsymbol{\theta} | \boldsymbol{S}_{k-L}, \ldots, \boldsymbol{S}_{k+L}). \tag{9}$$

It is well known that this non-linear least squares problem is non-convex [3]. Hence, it is viable to look for approximate solutions, possibly obtained in a greedy fashion.

Approaches like RIMAX [3] or Orthogonal Matching Pursuit (OMP) [13] have established that in many cases a careful greedy and iterative initialization can produce close to optimal results. The notion "iterative" refers to the approach of successively adding one path after the other, while "greedy" refers to a matched-filter approach during the search for a single new path.

a) Initialization To start the processing of the time-series $(\boldsymbol{S}_k)_{k \in \mathbb{N}}$ we essentially apply SAGE as presented in [14] for the model in (3) to get an initial guess for the parameters. One

Authorized licensed use limited to: NIST Virtual Library (NVL). Downloaded on July 14,2025 at 16:48:16 UTC from IEEE Xplore. Restrictions apply.

Data: input $\boldsymbol{S} \in \mathbb{C}^{m_{\mathrm{rx}} \times m_{\mathrm{t}}}$
Result: $\hat{P} \in \mathbb{N}$, $\hat{\boldsymbol{\gamma}} \in \mathbb{C}^{\hat{P}}$, $\hat{\boldsymbol{\tau}} \in \mathbb{R}^{\hat{P}}, \hat{\boldsymbol{\Omega}} \in (S^2)^{\hat{P}}$
Initialize $\hat{P} = 0$ and the residual $\boldsymbol{r} = \boldsymbol{S}$;
while *residual* $\boldsymbol{r}$ *still contains MPCs* **do**
  $\hat{P} \leftarrow \hat{P} + 1$;
  Apply a matched filter on $\boldsymbol{r}$ using (3) to find new MPC parameters $\hat{\tau}_{\hat{P}}$ and $\hat{\Omega}_{\hat{P}}$;
  Run least-squares to get the BLUE for $\hat{\boldsymbol{\gamma}}$;
  Run SAGE based on (3) to refine $\hat{\boldsymbol{\gamma}}$, $\hat{\boldsymbol{\tau}}$ and $\hat{\boldsymbol{\omega}}$;
  Update the residual $\boldsymbol{r} = \boldsymbol{S} - \boldsymbol{Z}(\hat{\boldsymbol{\gamma}}, \hat{\boldsymbol{\tau}}, \hat{\boldsymbol{\omega}})$;
end

Algorithm 1: *Interleaved execution of a matched filter and SAGE to produce an iterative greedy maximum likelihood estimator.*

Data: current window position k; window advance $W \in \mathbb{N}$; measured snapshots $(\boldsymbol{S}_{k-L}, \ldots, S_{k+L})$; estimates from prior window $\hat{\boldsymbol{\tau}}_{k-W}$, $\hat{\boldsymbol{\Omega}}_{k-W}$, $\hat{\dot{\boldsymbol{\tau}}}_{k-W}$, $\hat{\dot{\boldsymbol{\Omega}}}_{k}$
Result: $\hat{\boldsymbol{\gamma}}_k \in \mathbb{C}^{(2L+1)\times \hat{P}}$, $\hat{\boldsymbol{\tau}}_k \in \mathbb{R}^{\hat{P}}, \hat{\boldsymbol{\Omega}}_k \in (S^2)^{\hat{P}}$, $\hat{\dot{\boldsymbol{\tau}}}_k \in \mathbb{R}^{\hat{P}}, \hat{\dot{\boldsymbol{\Omega}}} \in (\mathbb{T}S^2)^{\hat{P}}$
Estimate $\hat{\boldsymbol{\gamma}}_k$ using least-squares;
Initialize

$$\hat{\boldsymbol{\tau}}_k \leftarrow \hat{\boldsymbol{\tau}}_{k-W} + \Delta t \cdot W \cdot \hat{\dot{\boldsymbol{\tau}}}_{k-W}, \hat{\dot{\boldsymbol{\tau}}}_k \leftarrow \hat{\dot{\boldsymbol{\tau}}}_{k-W}$$

$$\hat{\boldsymbol{\Omega}}_k \leftarrow \hat{\boldsymbol{\Omega}}_{k-W} + \Delta t \cdot W \cdot \hat{\dot{\boldsymbol{\Omega}}}_{k-W}, \hat{\dot{\boldsymbol{\Omega}}}_k \leftarrow \hat{\dot{\boldsymbol{\Omega}}}_{k-W}$$

Use SAGE based on (6) to refine the predicted value $\hat{\boldsymbol{\theta}}_k$ using $(\boldsymbol{S}_{k-L}, \ldots, S_{k+L})$;

Algorithm 2: *Prediction and refinement when moving from one window of snapshots to the next.*

common and simple approach for this is outlined in Algorithm 1. For more implementational details of Algorithm 1, see [3]. Note that given all other components of $\boldsymbol{\theta}_k$ except the complex path-weights $\boldsymbol{\gamma}_{k-\ell}, \ldots, \boldsymbol{\gamma}_{k+\ell}$, those weights can be estimated efficiently by means of linear least-squares and in case of colored Gaussian noise, this constitutes the Best Linear Unbiased Estimator (BLUE).

b) Sequential Estimation Further, we need an algorithm that successively moves us through the measurement campaign from one window of snapshots to another. In other words, given a window advance $W \geqslant 0$ and estimate $\hat{\boldsymbol{\theta}}_k$ based on the window of snapshots $\boldsymbol{S}_{k-L}, \ldots, \boldsymbol{S}_{k+L}$ we wish to estimate $\hat{\boldsymbol{\theta}}_{k+W}$ based on the data $\boldsymbol{S}_{k-L+W}, \ldots, \boldsymbol{S}_{k+L+W}$. We present one possible realization of such a procedure in Algorithm 2.

The core idea is to straightforwardly generalize SAGE as presented in [14] to the extended parameter $\boldsymbol{\theta}_k$ in (8) that also contains derivatives. We have implemented it using a matched filter, i.e. beamforming, to conduct the respective maximization step, of the Expectation Maximization (EM) algorithm. In this case we make use of the fact that given for instanced τ and $\dot{\tau}$, we can se

$$\boldsymbol{f}(\tau + \Delta t \cdot \ell \cdot \dot{\tau}) \quad \text{for} \quad \ell = -L, \ldots, +L$$

to get beamforming weights based on the current parameters such that they correspond to the snapshots $\boldsymbol{S}_{k-L}, \ldots, \boldsymbol{S}_{k+L}$.

c) Processing Pipeline The complete processing procedure is conducted as follows. We use Algorithm 1 to obtain the preliminary estimate, where the derivatives are initialized via $\hat{\dot{\boldsymbol{\tau}}}_L = \mathbf{0}$ and $\hat{\dot{\boldsymbol{\Omega}}}_L = \mathbf{0}$, which gives us the estimate $\hat{\boldsymbol{\theta}}_L$ according to (8). Then we run Algorithm 2 with $W = 0$ to refine $\hat{\boldsymbol{\theta}}_L$, now also estimating derivatives. Afterwards, we keep executing Algorithm 2 for some window advance $W > 0$ until all snapshots have been processed. In cases when $W > 1$ we can use linear interpolation and least-squares to get estimates for $\boldsymbol{\theta}_k$ for any k that we have skipped.

IV. Numerical Results

The numerical results we present rely on the measurement system described in [1], which excites the channel using a pre-distorted, i.e. optimized, Pseudo-Noise (PN) sequence being sent at $2\,\mathrm{Gbit\,s^{-1}}$ and is sampled at rate $16\,\mathrm{GHz}$. The TX is an 8×8 phased array optimized to produce an approximately uniform array response in terms of Direction of Departure (DoD). The RX uses four stacked 8×8 phased arrays, where a switched beamforming scheme increases the achievable measurement speed. In all the considered scenarios TX and RX are arranged in a quasi-monostatic configuration.

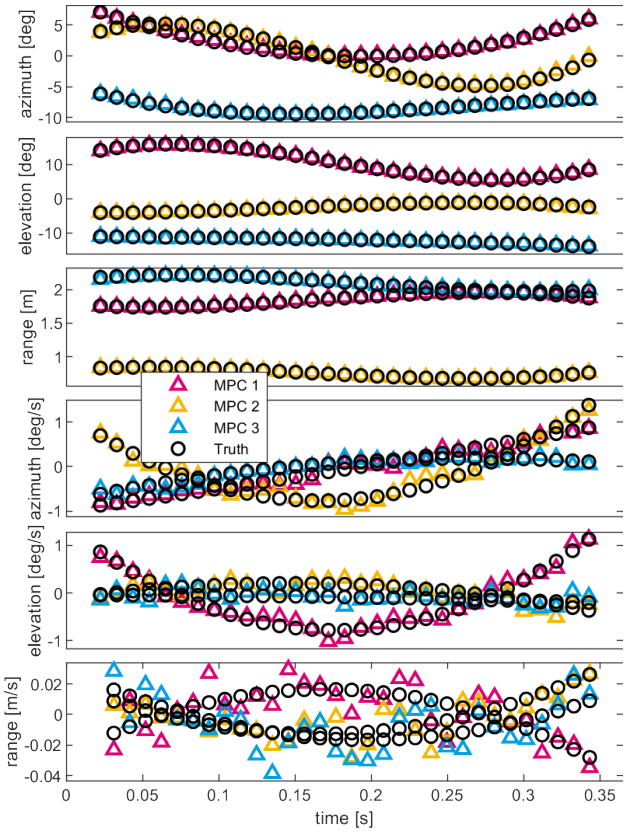

Fig. 1. *Ground truth (black) and estimated (colored) MPC parameters (top three plots) and the derivatives (bottom three) for synthetic data based on* (3) *using Algorithm 1 for the initialization and and Algorithm 2 for the processing of consecutive snapshots. The colored trajectories indicate that Algorithm 2 successfully associates MPCs estimates from adjacent snapshots.*

A. Synthetic Data

We first invoke the algebraic system model (3) for above system to generate the full and compressed data synthetically. We use 9 cubic splines to model the trajectories of the 3 time-variant MPCs, generate random independent circularly symmetric complex Gaussian path-weights, feed all into (2) and then add noise to $\boldsymbol{Y}$ to obtain a Signal-to-Noise Ratio (SNR) of $10\,\mathrm{dB}$ before applying the compression in (2). Note that choosing cubic splines introduces a model mismatch, since we locally apply a linear approximation in (6). We compress the data to $20\,\%$ of its original size by choosing $m_{\mathrm{rx}} = \lceil \sqrt{0.2} N_{\mathrm{rx}} \rceil$ and $m_{\mathrm{t}} = \lceil \sqrt{0.2} N_{\mathrm{t}} \rceil$. We set $L = 8$ to consider 17 consecutive windows for the local approximation and the construction of the matrices $\tilde{\boldsymbol{\Phi}}_\ell$ and $\tilde{\boldsymbol{\Psi}}_\ell$. Additionally, for Algorithm 2 we choose the window advance as $W = 3$.

The results in Fig. 1 showcase that for perfect system knowledge the proposed estimation and tracking of closely spaced and partially intersecting MPCs is possible, even though the cubic MPC dynamics are not exactly captured by the local linear motion model (6). Further, the estimation of $\dot{\boldsymbol{\tau}}$ and $\dot{\boldsymbol{\Omega}}$ is following the quadratic trajectories of the splines' derivatives. As is common for estimating derivatives

Authorized licensed use limited to: NIST Virtual Library (NVL). Downloaded on July 14,2025 at 16:48:16 UTC from IEEE Xplore. Restrictions apply.

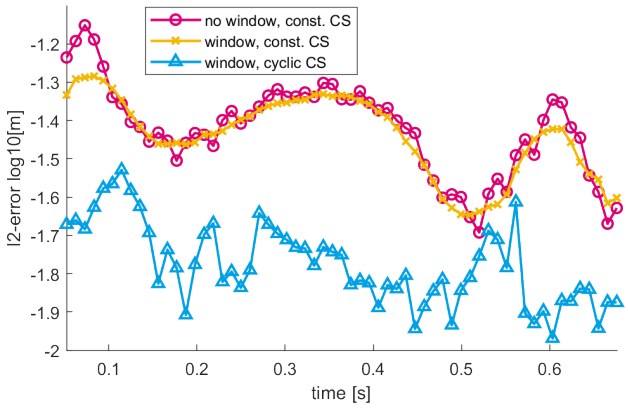

Fig. 2. *Comparison of the MSE for MPC estimation between "plain vanilla" CS (no window, const. CS, red), the proposed temporally consistent model (window, const. CS, yellow) and the proposed complete sensing pipeline (window, cyclic CS, blue).*

from noisy data, these estimates show a greater fluctuation around their expected value than the parameters themselves.

Next, we present numerical evidence that first the parametric model for a window of multiple snapshots makes the estimated MPCs temporally more consistent and second that the combination with the proposed cyclic compression scheme improves the accuracy of the processing. To this end, we conduct three different sensing and estimation scenarios using the same MPCs as ground truth. In all cases, we choose an SNR of $10\,\mathrm{dB}$, keep the number of MPCs fixed at $P = 2$, use $W = 1$ as the windowing advance and we generate 60 snapshots that are each spaced $10.4\,\mathrm{ms}$ apart. In the first scenario, we choose only one pair of compression matrices both for the spatial and delay domain and set $\mathbf{\Phi}_k = \tilde{\mathbf{\Phi}}_\mathbf{1}$ and $\mathbf{\Psi}_k = \tilde{\mathbf{\Psi}}_\mathbf{1}$ respectively. Further, we set $L = 0$, which essentially results in a data model (3), where the rates of change of the parameters are not identifiable, hence we also do not estimate them in this case. In the second scenario, we alter the previous setting, by choosing $L = 3$ and keeping the rest as before. This allows us to obtain estimates for the rates of change, but each snapshot is still compressed by the same matrices $\tilde{\mathbf{\Phi}}_\mathbf{1}$ and $\tilde{\mathbf{\Psi}}_\mathbf{1}$. In the third scenario, we also make use of the proposed cyclic compression scheme and define $2L + 1 = 7$ independently generated $\tilde{\mathbf{\Phi}}_{\boldsymbol{\ell}}$ and $\tilde{\mathbf{\Psi}}_{\boldsymbol{\ell}}$ with $\ell = 1, \ldots, 2L + 1$. We would like to note that in case of $L = 0$ it is irrelevant, if we use the same or different compression matrices, since as long adjacent snapshots are not "connected" by a data, on average each instance of Φ_k or $\mathbf{\Psi}_k$ delivers the same performance in terms of estimation quality.

In Fig. 2 we compare the resulting estimation errors by converting delay to range and then use the AoA to transform the estimates and the ground truth to Euclidean space, where distances are easy to calculate in meters. As we have argued before, the introduction of the temporal consistency smoothens out the estimated MPCs, visible from that fact that "no window, const. CS" shows more fluctuation than "window, const. CS". Finally, using the cyclic compression scheme, i.e. "window, cyclic CS", substantially reduces the estimation error compared to the constant compression. So although the overall compression rate stays the same, by using $2L + 1 = 7$ compression matrices instead of 1, the estimation performance can be improved, when combined with the data model that spans multiple snapshots.

B. Measurement Data

Last, we present controlled numerical experiments on real measurement data, obtained with the system described in Section I, where the ground truth is inferable from the measurement setup. To this end, we fix one metal plate on a stationary tripod, where another metal plate is attached to a movable cart at elevation 0° and azimuth -18° at distance $2\,\mathrm{m}$. During the measurements a second plate at elevation 0° and azimuth 5° is moving on the cart towards the receiver while

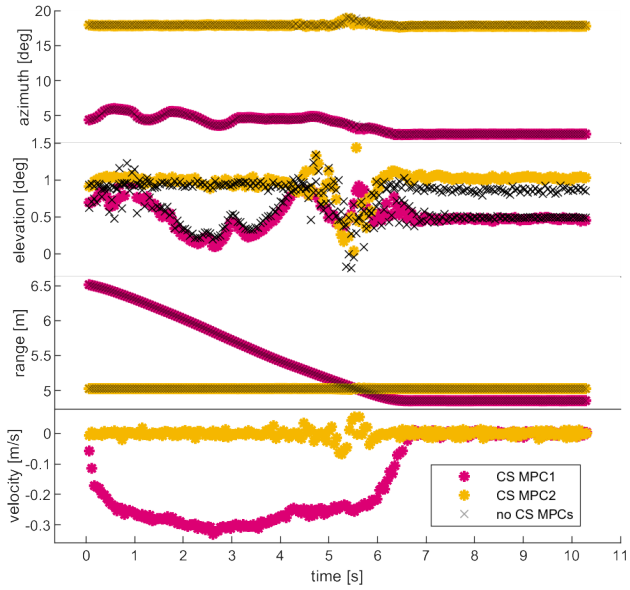

Fig. 3. *Comparison between estimates based on compressed data (colored) and estimates obtained from full data (black) for one fixed and one moving metal plate. The bottom plot shows the rate of change for the range based on* $\hat{\dot{\boldsymbol{\tau}}}$.

being aligned in such a way that the plane wave is traveling from broadside TX and is received by the broadside of RX. After a few seconds the cart stops. The data is digitized and stored at Nyquist rate and then compressed offline in order to allow flexible exchange of different compression schemes and their comparison. In this specific case presented we choose $L = 5$, $W = 5$, $m_{\mathrm{rx}} = \lceil \sqrt{0.3} N_{\mathrm{rx}} \rceil$ and $m_{\mathrm{t}} = \lceil \sqrt{0.1} N_{\mathrm{t}} \rceil$ for a total compression to approximately $17\,\%$ of the original size.

Due to an unknown ground truth, we compare the estimates from the compressed data with the estimates produced by the conventional SAGE as presented in [14] applied to the full data. The results in Fig. 3 show a good agreement between the estimates in all three parameter domains. Only the crossing in range of the two metal plates marginally disturbs the estimated MPCs. Interestingly, the range velocity at the bottom of Fig. 3 of around $-0.3\,\mathrm{m\,s^{-1}}$ matches well with the trajectory of the delay.

V. Conclusion & Outlook

From the presented results we conclude that incorporating a local temporally coherent model contributes to more stable estimates of specular MPCs. In our case this is enabled by including rates of change into the parameter space and the parametric model. Further, we show how to design a parameter estimation routine based on CLEAN and SAGE that allows the estimation of these parameters. Not only does the temporally consistent model provide more stable MPC estimates, it also allows to employ a cyclic compression scheme that is able to retrieve more information from the signal than using a constant compression matrix. As a consequence the proposed CS approach can deliver around 4 times lower estimation errors than previous compression methods.

To extend the current proposal, first, the compression should be executed directly in the measurement device and we aim at showing a trigger-based spatial subsampling in future works. One can make use of compression matrices that have a fast transform to speed up the estimation routine [15]. One could aim at refining the sensing scheme by employing an optimization that tunes the compression specifically for the system model [16]. Finally, the birth and death process of the MPCs has to be accounted for in Algorithm 2. For instance statistical tests can be used to estimate the model order P while processing the snapshots.

Authorized licensed use limited to: NIST Virtual Library (NVL). Downloaded on July 14,2025 at 16:48:16 UTC from IEEE Xplore. Restrictions apply.

References

[1] D. Caudill, J. Chuang, S. Y. Jun, C. Gentile, and N. Golmie, "Real-time mmwave channel sounding through switched beamforming with 3-d dual-polarized phased-array antennas," *IEEE Transactions on Microwave Theory and Techniques*, no. 11, 2021.

[2] J. Fessler and A. Hero, "Space-alternating generalized expectation-maximization algorithm," *IEEE Transactions on Signal Processing*, no. 10, 1994.

[3] A. Richter, "Estimation of radio channel parameters," 2005.

[4] M. Haardt, R. Thomä, and A. Richter, "Multidimensional high-resolution parameter estimation with applications to channel sounding," English, in *High-Resolution and Robust Signal Processing*, Y. Hua, Ed. 2003.

[5] E. J. Candès and C. Fernandez-Granda, "Super-resolution from noisy data," *J. Fourier Anal. Appl.*, no. 6, 2013.

[6] R. Heckel and M. Soltanolkotabi, "Generalized line spectral estimation via convex optimization," *IEEE Trans. Inf. Theory*, no. 6, 2017.

[7] M. Ibrahim, F. Romer, R. Alieiev, G. Del Galdo, and R. S. Thoma, "On the estimation of grid offsets in {cs}-based direction-of-arrival estimation," in *2014 IEEE International Conference on Acoustics, Speech and Signal Processing (ICASSP)*, IEEE, 2014.

[8] M. Ibrahim, W. Al-Aqqad, F. Romer, M. Kaske, S. Semper, R. Thoma, and G. Del Galdo, "Compressive spatial channel sounding," in *12th European Conference on Antennas and Propagation (EuCAP 2018)*, Institution of Engineering and Technology, 2018.

[9] J. Salmi, A. Richter, and V. Koivunen, "Detection and tracking of mimo propagation path parameters using state-space approach," *IEEE Transactions on Signal Processing*, no. 4, 2009.

[10] M. Inami, N. Kikuma, and K. Sakakibara, "Performance improvement of doa estimation using compressed sensing by sage algorithm," in *2019 International Symposium on Antennas and Propagation (ISAP)*, 2019.

[11] J. Rodríguez-Fernández, N. González-Prelcic, and R. W. Heath, "A compressive sensing-maximum likelihood approach for off-grid wideband channel estimation at mmwave," in *2017 IEEE 7th International Workshop on Computational Advances in Multi-Sensor Adaptive Processing (CAMSAP)*, 2017.

[12] S. Foucart and H. Rauhut, *A Mathematical Introduction to Compressive Sensing*. Springer New York, 2013.

[13] Y. Pati, R. Rezaiifar, and P. Krishnaprasad, "Orthogonal matching pursuit: Recursive function approximation with applications to wavelet decomposition," in *Proceedings of 27th Asilomar Conference on Signals, Systems and Computers*, IEEE Comput. Soc. Press, 1993.

[14] B. Fleury, M. Tschudin, R. Heddergott, D. Dahlhaus, and K. Ingeman Pedersen, "Channel parameter estimation in mobile radio environments using the sage algorithm," *IEEE Journal on Selected Areas in Communications*, no. 3, 1999.

[15] C. W. Wagner, S. Semper, and J. Kirchhof, "Fastmat: Efficient linear transforms in python," *SoftwareX*, 2021.

[16] S. Pawar, S. Semper, and F. Romer, "Combining matrix design for 2D DoA estimation with compressive antenna arrays using stochastic gradient descent," in *ICASSP 2019 - 2019 IEEE International Conference on Acoustics, Speech and Signal Processing (ICASSP)*, IEEE, 2019.

Authorized licensed use limited to: NIST Virtual Library (NVL). Downloaded on July 14,2025 at 16:48:16 UTC from IEEE Xplore. Restrictions apply.